

# Evolution and structure of sink-flow turbulent boundary layers

By M. B. JONES<sup>1</sup>, IVAN MARUSIC<sup>2</sup> AND A. E. PERRY<sup>1</sup>

<sup>1</sup>Department of Mechanical and Manufacturing Engineering, University of Melbourne, Parkville,  
Victoria 3052, Australia

<sup>2</sup>Department of Aerospace Engineering and Mechanics, University of Minnesota,  
Minneapolis, MN 55455, USA

(Received 26 February 1999 and in revised form 4 June 2000)

An experimental and theoretical investigation of turbulent boundary layers developing in a sink-flow pressure gradient was undertaken. Three flow cases were studied, corresponding to different acceleration strengths. Mean-flow measurements were taken for all three cases, while Reynolds stresses and spectra measurements were made for two of the flow cases. In this study attention was focused on the evolution of the layers to an equilibrium turbulent state. All the layers were found to attain a state very close to precise equilibrium. This gave equilibrium sink flow data at higher Reynolds numbers than in previous experiments. The mean velocity profiles were found to collapse onto the conventional logarithmic law of the wall. However, for profiles measured with the Pitot tube, a slight ‘kick-up’ from the logarithmic law was observed near the buffer region, whereas the mean velocity profiles measured with a normal hot wire did not exhibit this deviation from the logarithmic law. As the layers approached equilibrium, the mean velocity profiles were found to approach the pure wall profile and for the highest level of acceleration  $\Pi$  was very close to zero, where  $\Pi$  is the Coles wake factor. This supports the proposition of Coles (1957), that the equilibrium sink flow corresponds to pure wall flow. Particular interest was also given to the evolutionary stages of the boundary layers, in order to test and further develop the closure hypothesis of Perry, Marusic & Li (1994). Improved quantitative agreement with the experimental results was found after slight modification of their original closure equation.

---

## 1. Introduction

A sink-flow turbulent boundary layer is one with a pressure gradient that follows that of a two-dimensional potential sink. Consider a sink flow as shown schematically in figure 1;  $U_0$  is the reference free-stream velocity at some conveniently selected origin (i.e. the beginning of the boundary layer) and at  $x = L$  there exists a potential sink of strength  $Q$ , where  $x$  is the streamwise coordinate. From continuity and neglecting boundary layer displacement effects the local free-stream velocity  $U_1$  can be shown to be given by

$$\frac{U_1}{U_0} = \frac{1}{1 - x/L}. \quad (1.1)$$

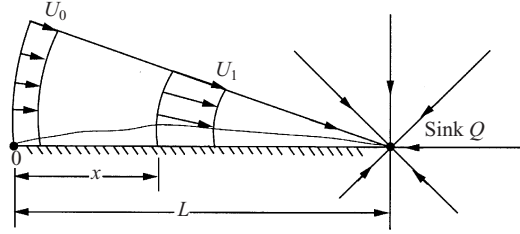


FIGURE 1. Sink flow.

A sink flow can be uniquely characterized by the acceleration parameter  $K$  which is defined as

$$K = \frac{\nu}{U_1^2} \frac{dU_1}{dx} \quad (1.2)$$

and for a sink flow  $K$  is a positive constant and is given by

$$K = \frac{\nu}{U_0 L} \quad (1.3)$$

where  $\nu$  is the kinematic viscosity of the fluid.

In the literature, the sink-flow boundary layer often appears in discussions relating to equilibrium concepts. This is because it is the only smooth wall boundary layer that satisfies the required conditions for precise equilibrium and this was first shown by Townsend (1956) and later by Rotta (1962). Here the definition of a precise equilibrium layer is one where the mean defect velocity profiles and Reynolds stress profiles are invariant with the streamwise coordinate, when they are scaled with the correct velocity and length scales. Coles (1957) also identified this unique equilibrium property of the sink flow. Further he made an important contribution by proposing that the sink flow at equilibrium corresponds to pure wall flow, that is  $\Pi = 0$ , where  $\Pi$  is the Coles wake strength factor. Coles (1957) provides several arguments to support his hypothesis but there is no rigorous proof which shows  $\Pi = 0$  for the sink flow at equilibrium.

The unique properties of the sink flow make it an interesting layer to study. Furthermore, it represents a favourable pressure gradient which is clearly defined and can be produced simply in the laboratory as flow between converging plane surfaces. Since a major motivation of the study was to test and further develop the closure hypothesis proposed by Perry, Marusic & Li (1994) the sink flow provided a convenient experimental test case. Hence the experiments serve not only to provide information about the equilibrium state but also show the details of the evolution.

Limited experimental data have been taken in sink flows and much of what is available is confined to low Reynolds number layers with the emphasis often being on studying the relaminarization problem. Herring & Norbury (1967) were perhaps the first to take measurements in a sink flow. They took mean flow measurements in favourable pressure gradients of two different strengths. While they did not identify their flows as being sink flows, a review of their pressure gradient reveals that they follow very closely sink flows with approximate acceleration parameters  $K = 1.2 \times 10^{-7}$  and  $K = 1.8 \times 10^{-7}$ . Unfortunately the length of development they observed was fairly limited, their last measuring stations being at  $x/L = 0.25$  for the lower  $K$  value and  $x/L = 0.38$  for the higher  $K$  value.

A more detailed experimental study of the sink flow was undertaken by Jones & Launder (1972). They studied it at three different levels of acceleration:  $K = 1.5 \times 10^{-6}$ ,

$2.5 \times 10^{-6}$  and  $3.0 \times 10^{-6}$ . These levels of acceleration are characterized by low Reynolds number boundary layers, their Reynolds numbers based on momentum thickness were in the range  $300 < R_\theta < 700$ , here  $R_\theta = U_1 \theta / \nu$  where  $\theta$  is the momentum thickness. They took both mean and turbulence measurements and the streamwise extent of their measurements corresponded to  $x/L \approx 0.55$ . From their results they concluded that the flows with the two lowest values of  $K$  had reached equilibrium. Their non-dimensional mean velocity profiles were found to have higher velocities than the standard logarithmic law of the wall and the amount of excess increased with  $K$ . In fact for the two higher values of  $K$  the profiles showed no discernible universal logarithmic region.

Numerical simulations of sink-flow boundary layers, at equilibrium, were performed by Spalart (1986). The values of the acceleration parameter chosen for Spalart's simulations corresponded to those of Jones & Launder (1972) and hence represent low Reynolds number layers. The agreement with Jones & Launder's (1972) results was generally found to be good. However at the highest acceleration ( $K = 3.0 \times 10^{-6}$ ) Spalart found that no long-time turbulent solution could be generated. The mean velocity profiles showed similar behaviour to those of Jones & Launder (1972) in that as  $K$  was increased the profiles were displaced up from the standard log law and for the simulation at the highest  $K$  no log law was observed.

The results presented in this paper are from experiments in sink flows at three levels of acceleration:  $K = 2.70 \times 10^{-7}$ ,  $3.59 \times 10^{-7}$  and  $5.39 \times 10^{-7}$ , which produced significantly higher Reynolds numbers at equilibrium than previous studies ( $1800 < R_\theta < 3000$ ). The evolution of the boundary layers from initial arbitrary conditions was studied in detail and this allowed comparisons with the predicted solutions obtained using the closure hypothesis of Perry *et al.* (1994). It is also important to capture the equilibrium state of the layers, since the data may serve to reveal the structure of pure wall flow. Measurements were therefore taken up to a maximum streamwise station which corresponded to  $x/L = 0.65$  and it was found that equilibrium was approached at  $x/L \approx 0.60$ .

### 1.1. Closure hypothesis

As has already been mentioned a major motivation of the study was to test the closure hypothesis of Perry *et al.* (1994); therefore a short review of it will be given here.

An essential feature of the closure hypothesis is the expression for the total shear stress profile. This was derived by Perry *et al.* (1994) assuming the mean velocity profile is given by a Coles (1956) logarithmic law of the wall and law of the wake formulation,

$$\frac{U}{U_\tau} = \frac{1}{\kappa} \ln \left[ \frac{z U_\tau}{\nu} \right] + A + \frac{\Pi}{\kappa} W_c[\eta, \Pi]. \quad (1.4)$$

In the above  $U$  is the mean streamwise velocity,  $U_\tau$  is the wall shear velocity,  $\kappa$  is the Kármán constant,  $A$  is the universal smooth wall constant,  $\Pi$  is the Coles wake factor,  $W_c$  is the Coles wake function and  $\eta = z/\delta_c$ , where  $\delta_c$  is the boundary layer thickness and  $z$  is the wall-normal coordinate. It should be stated at the outset that the logarithmic law of the wall is assumed valid right down to the wall, i.e. the viscous sublayer and buffer zone are being neglected. It has been found (e.g. Perry *et al.* 1994) that the inclusion of these zones has a negligible effect on the computation of total shear stress and on the momentum and displacement thicknesses, see Appendix B. Hence the effect on the overall momentum balance is small when these zones

are neglected, for practical ranges of Reynolds number. Considering two-dimensional flow in the mean, Perry *et al.* (1994) use the mean momentum equation and continuity equation in conjunction with (1.4) to derive an expression for the total shear stress which is given by

$$\frac{\tau}{\tau_0} = f_1[\eta, \Pi, S] + g_1[\eta, \Pi, S]\zeta + g_2[\eta, \Pi, S]\beta. \quad (1.5)$$

In (1.5)  $\tau$  is the local shear stress,  $\tau_0$  is the wall shear stress,  $S = U_1/U_\tau$ ,  $\beta$  is the Clauser (1956) pressure gradient parameter given by

$$\beta = \frac{\delta^*}{\tau_0} \frac{dp_1}{dx}, \quad (1.6)$$

where  $\delta^*$  is the displacement thickness,  $p_1$  is the free-stream static pressure and  $\zeta$  represents a wake strength gradient parameter given by

$$\zeta = S\delta_c \frac{d\Pi}{dx}. \quad (1.7)$$

The quantities  $f_1[\eta, \Pi, S]$ ,  $g_1[\eta, \Pi, S]$  and  $g_2[\eta, \Pi, S]$  are known analytical functions (found using *Mathematica* or *Maple*) and their forms depend on the wake function used in (1.4).

When deriving (1.5) Perry *et al.* (1994) used the Lewkowicz (1982) wake function

$$W_c[\eta, \Pi] = 2\eta^2(3 - 2\eta) - \frac{1}{\Pi}\eta^2(1 - \eta)(1 - 2\eta), \quad (1.8)$$

where the polynomial pre-multiplied by  $1/\Pi$  is included to ensure that (1.4) has zero gradient at  $z = \delta_c$ . Jones (1998) refers to this as the corner function and, strictly, this function should not be included in the wake function. Further it was found that inclusion of this corner function resulted in a poor fit of (1.4) to profiles that had low values of  $\Pi$ . Therefore Jones (1998) used a logarithmic law of the wall and law of the wake given by<sup>†</sup>

$$\frac{U}{U_\tau} = \underbrace{\frac{1}{\kappa} \ln \left[ \frac{zU_\tau}{\nu} \right] + A}_{\text{Pure wall flow}} \quad \underbrace{-\frac{1}{3\kappa}\eta^3 + \frac{\Pi}{\kappa} 2\eta^2(3 - 2\eta)}_{\text{Pure wake component}} \quad (1.9)$$

to derive the functions  $f_1[\eta, \Pi, S]$ ,  $g_1[\eta, \Pi, S]$  and  $g_2[\eta, \Pi, S]$  appearing in (1.5) and these forms are used in all the following analysis. The term  $-\eta^3/(3\kappa)$  included in (1.9) is required to give the correct behaviour at the edge of the layer and this is particularly important for profiles where  $\Pi \rightarrow 0$ . Further in (1.9), the wake function  $W_c$  is now more correctly a function of  $\eta$  alone and this functional form was first proposed by Moses (1964). It should be noted that mean-flow parameters,  $S$ ,  $\Pi$ , and  $\delta_c$ , were systematically determined based on a parametric fit of (1.9) to data. The method used was to find  $S$  from the Clauser chart, measure the maximum deviation from the logarithmic law which from (C 2) gives  $\Pi$  and then  $\delta_c$  is found using (A 3) and (B 1). These equations are found in the Appendices; note that alternative methods for finding the above parameters could be devised. For the purpose of analysis the log-law constants assumed the values  $\kappa = 0.41$ , and  $A = 5.0$ .

<sup>†</sup> This decomposition was suggested to the authors by Professor D. Coles of GALCIT, Caltech (private communication).

An important feature of the functions  $f_1[\eta, \Pi, S]$ ,  $g_1[\eta, \Pi, S]$  and  $g_2[\eta, \Pi, S]$  is that they become independent of  $S$  as  $S \rightarrow \infty$ . Using this Perry *et al.* (1994) formulated the hypothesis that a given shear stress profile at finite  $S$  will match a unique shear stress profile at  $S = \infty$ . Initially Perry *et al.* (1994) considered the closure hypothesis for approximate equilibrium layers, where an approximate equilibrium layer is defined as one which exhibits similarity in the mean defect profiles only and hence  $\zeta = 0$  but the shear stress profiles are approximately matched for a given  $\Pi$  for all  $S$  (this is consistent with eddy viscosity formulations). For such a class of layers Perry *et al.* (1994) matched the shear stress profiles at  $\eta = 0.4$  which results in the equation

$$\beta[\Pi, S] = \frac{-f_1[0.4, \Pi, S] + f_1[0.4, \Pi, \infty] + g_2[0.4, \Pi, \infty]\beta_{ae}[\Pi]}{g_2[0.4, \Pi, S]}. \quad (1.10)$$

The function  $\beta_{ae}[\Pi]$  represents the asymptotic form of  $\beta$  for  $S \rightarrow \infty$  for the restricted case of approximate equilibrium layers and it is still to be determined from experimental data. However for the purpose of computations Perry *et al.* (1994) used the relationship

$$\beta_{ae}[\Pi] = \left( 0.030 \left( \frac{C_2[\Pi]}{C_1[\Pi]} \right)^2 - 1.25 \right), \quad (1.11)$$

which was proposed by Green, Weeks & Brooman (1973); here  $C_1[\Pi]$  and  $C_2[\Pi]$  are functions of  $\Pi$  that are given in Appendix A.

The equations that govern the evolution of an approximate equilibrium boundary layer which is two-dimensional in the mean can be generated from the momentum integral equation in conjunction with the log-law of the wall and law of the wake. The momentum integral equation for two-dimensional flow in the mean is given by

$$\frac{d\theta}{dx} + \frac{(H+2)\theta}{U_1} \frac{dU_1}{dx} = C'_f/2 \quad (1.12)$$

where  $C'_f$  is the local skin friction coefficient and  $H = \delta^*/\theta$ . Using (1.9) expressions for the mean integral parameters can be generated which when substituted into (1.12) gives the evolution equation

$$SE[\Pi] \exp[\kappa S] \frac{1}{\chi} \frac{dS}{dR_x} = R[S, \beta, \Pi], \quad (1.13)$$

where  $\chi = U_1/U_0$ ,  $R_x = xU_0/\nu$  and the functional forms of  $E[\Pi]$  and  $R[S, \beta, \Pi]$  are given in Appendix A. Using the log-law of the wall and law of the wake given by (1.9),  $\beta$  can be expressed in the form of an auxiliary equation:

$$S^2 E[\Pi] \exp[\kappa S] \frac{1}{\chi^2} \frac{d\chi}{dR_x} = -\frac{\beta}{C_1[\Pi]}. \quad (1.14)$$

It is assumed that the evolution equation can be applied to flows where  $\Pi$  is allowed to vary slowly with  $x$  provided the parameter  $\zeta$  has a negligible effect on the shear stress profiles, i.e.

$$\frac{g_1[\eta, \Pi, S]\zeta}{f_1[\eta, \Pi, S] + g_2[\eta, \Pi, S]\beta} \ll 1 \quad (1.15)$$

and such layers are referred to as quasi-equilibrium layers, to which the sink flow is considered to belong, before it finally reaches precise equilibrium. Hence to solve the evolution of such layers the effect of the parameter  $\zeta$  is neglected and the evolution equation (1.13) can be solved by using the auxiliary equation (1.14) in conjunction

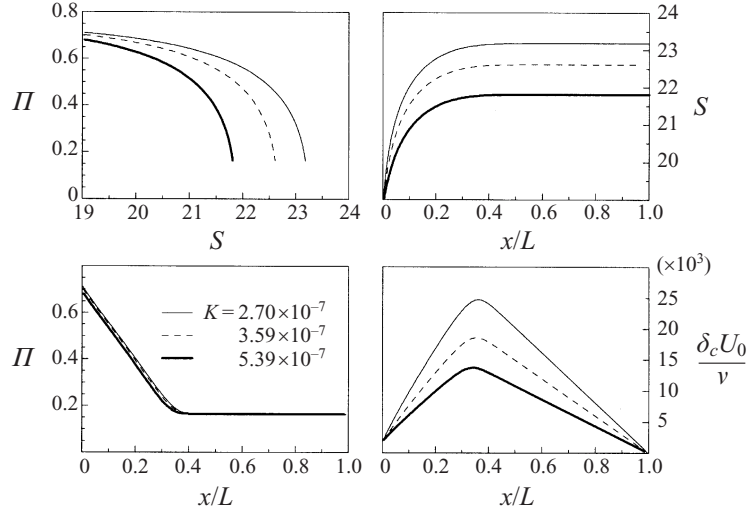


FIGURE 2. Evolution of mean flow parameters for sink flow, using the closure hypothesis of Perry *et al.* (1994), after Jones (1998).

with the closure equation obtained using (1.10) and (1.11). Perry *et al.* (1994) did this for layers developing under zero pressure gradient, sink-flow pressure gradient and source-flow pressure gradient, where source flow is defined by a constant negative value of  $K$ . Jones (1998) repeated these calculations for sink flows with acceleration levels of  $K = 2.70 \times 10^{-7}$ ,  $3.59 \times 10^{-7}$  and  $5.39 \times 10^{-7}$ , and the evolution of  $S$ ,  $\Pi$ , and  $\delta_c U_0/\nu$  according to these calculations are given in figure 2. For the purpose of these calculations the initial conditions have been specified by setting  $S_0 = 19$ , where  $S_0$  denotes the value of  $S$  at  $R_x = 0$ . This value of  $S_0$  is typical of layers soon after transition and of sufficient Reynolds number to have a log law. Once  $S_0$  is chosen all other initial conditions are fixed; this is a consequence of neglecting the parameter  $\zeta$  which constrains the solution to quasi-equilibrium.

## 2. Apparatus and experimental techniques

Experiments were performed in an open-return blower wind tunnel. The important features of the tunnel are a settling chamber containing honeycomb and five screens followed by a contraction with area ratio of 8.9 : 1 which leads into an initial working section area 940 mm wide by 375 mm high with a working section length of 4.2 m.

Details of the working section are shown in figure 3. The smooth acrylic floor of the working section provides the ‘smooth wall’ on which the boundary layer develops. The trip wire was placed at  $x = 0$  arbitrarily and the diameter  $d$  of the trip wire was chosen so that  $U_1 d/\nu$  fell within the range suggested by Erm & Joubert (1991) to give a correctly stimulated boundary layer. The pressure gradient for all experiments was controlled by a straight rigid ceiling hinged at the beginning of the working section.

The coefficient of pressure is given by

$$C_p = \frac{p_1 - p_0}{p_t - p_0} = 1 - \left( \frac{U_1}{U_0} \right)^2 \quad (2.1)$$

where  $p_0$  is the reference static pressure,  $p_1$  is the free-stream static pressure  $U_0$  is the reference free-stream velocity and  $p_t$  is the reference total pressure. For a sink flow

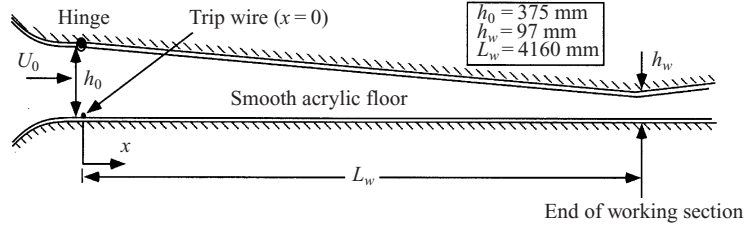


FIGURE 3. Working section geometry.

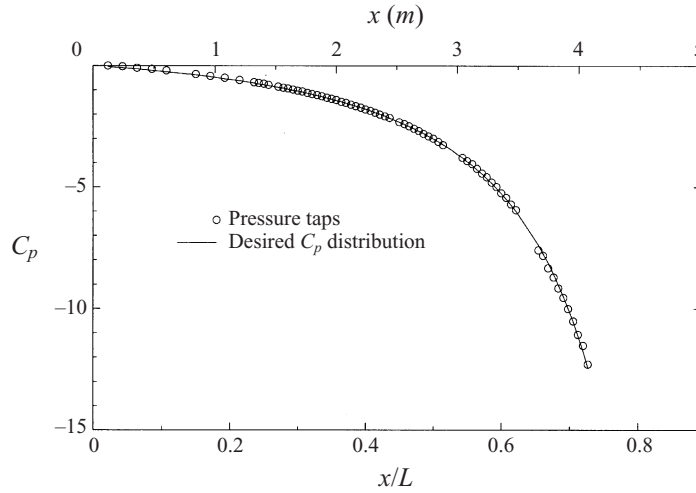


FIGURE 4. Streamwise pressure distribution.

assuming the boundary layer displacement effects are negligible, continuity gives the coefficient of pressure along the wall as

$$C_p = 1 - \frac{1}{(1 - x/L)^2}. \quad (2.2)$$

The  $C_p$  distribution, as measured by wall tappings for a given reference velocity, is shown in figure 4 and is seen to fit the desired  $C_p$  distribution (2.2) well. From a curve fit of (2.2) to the data the parameter  $L$  was found to be given by  $L = 5.60$  m. The  $C_p$  distribution shown in figure 4 was measured with a reference velocity corresponding to  $U_0 = 10 \text{ m s}^{-1}$ . However it was found from cursory checks that the distribution was invariant with Reynolds number (i.e. with  $U_0$ ). The geometry of the tunnel, and hence the  $C_p$  distribution, was held fixed for all flows and the reference velocity  $U_0$  varied in order to obtain the range of acceleration parameters  $K$  to be investigated. The nominal reference velocities were  $U_0 = 10.0, 7.5$  and  $5.0 \text{ m s}^{-1}$  which correspond to acceleration strengths  $K = 2.70 \times 10^{-7}, 3.59 \times 10^{-7}$  and  $5.39 \times 10^{-7}$  respectively. However to ensure constant  $K$  was maintained (i.e. constant Reynolds number), for a given flow case,  $U_0$  was adjusted to account for daily variations in fluid viscosity.

To check whether the flow could be considered two-dimensional in the mean, traverses were taken over a spanwise distance of 500 mm centred about the measuring station at a streamwise location  $x = 1200$  mm. Two traverses were performed: one in the free stream and one at a representative level within the boundary layer. For both traverses  $V/U$  is less than  $\pm 0.005$  and there is no preferred slope in the variation.

Here  $V$  is the mean spanwise component of velocity. It was also found that the variation in  $U$  was less than  $\pm 0.005$  of the average  $U$  velocity across the span.

A MKS Baraton 170M-6C manometer with a type 310BH-1 sensor was used to measure all pressure differences. A Pitot-static tube was used for mean-flow measurements. The total tube had an external diameter of  $d = 1.00$  mm and the static tube had an external diameter of 2.00 mm. The Pitot tube was corrected for the effect of shear using the MacMillan (1956) correction, which gives  $\delta_1/d = 0.15$ , where  $\delta_1$  is the effective location of the Pitot tube above its centreline. The wall shear velocity  $U_\tau$  was determined using two different methods: the Clauser chart and the Preston tube. The Clauser chart values were found to agree better with momentum balances and therefore all results presented use the values of  $U_\tau$  calculated from the Clauser chart.

Constant-temperature hot-wire anemometers were used for the measurement of turbulence quantities. The design of these anemometers is given in Perry (1982) and Perry & Morrison (1971*a*). Both normal-wire and cross-wire probes were used. The normal wire was used in preference to the cross-wire for the measurement of streamwise turbulence intensities and streamwise spectra, since it allows closer wall readings and reduces any errors associated with the effect of shear. The probes were mounted in 4 mm diameter tubing. The tubing was supported in a chuck that allowed accurate rotation through  $90^\circ$  and this enabled measurements to be taken in both the  $U, W$  and  $U, V$  planes when the cross-wire was used. The prong tip separation on all probes was 3.0 mm and the sensors were platinum Wollaston wire, etched to a length of 1.0 mm with a diameter of  $5\ \mu\text{m}$ . For the cross-wire probes the wires were attached at  $\pm 45^\circ$  to the streamwise direction and the wires were separated by a distance of 1.0 mm.

The Pitot-static and hot-wire signals were sampled by an Analog Devices RTI-860 data acquisition board installed in a SKAI 386 IBM compatible personal computer. Using 12-bit resolution the board was capable of sampling four channels simultaneously with a maximum sampling rate of 50 kHz per channel.

The dynamic calibration of Perry & Morrison (1971*b*) together with a nonlinear static calibration was used to calibrate all hot wires and for a comprehensive account of this technique the reader is referred to Perry (1982). When measuring broadband turbulence intensities the hot-wire signals were low-pass filtered at a cut-off frequency of 20 kHz, then bursts of 8000 samples were taken at a sampling frequency of 200 Hz. To get convergence of the data to within 0.5% four bursts were taken at each  $z$  coordinate. For spectra measurements, uncalibrated hot wires were used. In order to improve the frequency bandwidth of the spectrum the signals were sampled at three different sampling frequencies: 500 Hz, 5 kHz and 40 kHz. Using 8-pole Butterworth filters the signals were low-pass filtered at 0.4 times the respective sampling frequencies, thus avoiding aliasing when taking discrete Fourier transforms. For measurements using normal wires, 25 bursts of 2048 samples were taken while for cross-wire measurements, 100 bursts of 2048 samples were taken. The higher number of bursts for the cross-wire was to ensure convergence of the cross-power spectra.

### 3. Mean flow results

For each flow case, mean profiles at 20 streamwise stations were measured, from stations  $x = 400$  to 3620 mm. Representative mean velocity profiles for each flow case are shown in figure 5. Beyond the buffer region ( $zU_\tau/\nu \approx 100$ ) the profiles are well described by the logarithmic law of the wall and law of the wake given in (1.9).

The values of  $U_\tau$ ,  $\Pi$  and  $\delta_c$  were determined based on a parametric curve fit of



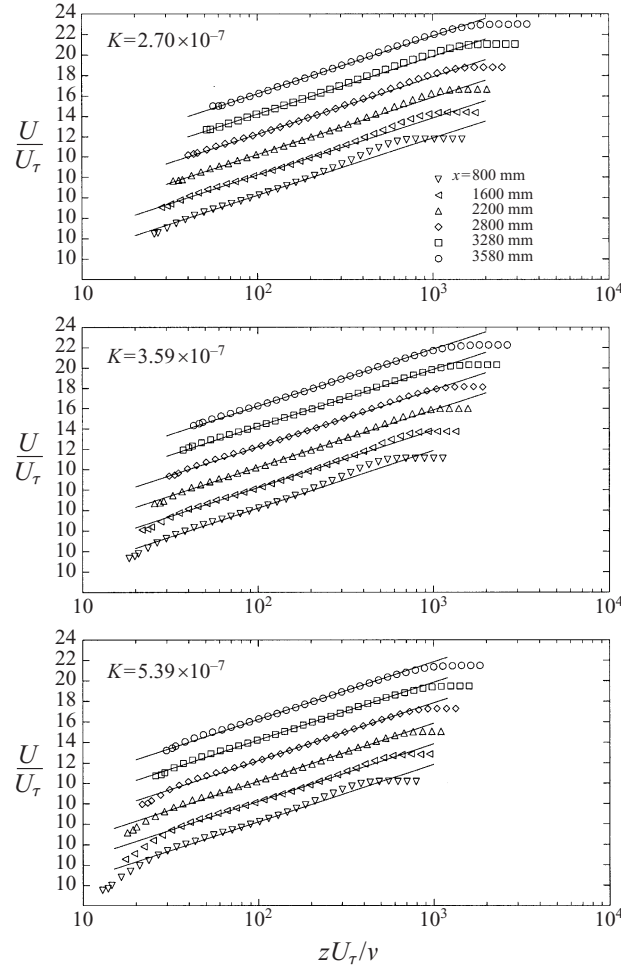


FIGURE 5. Mean velocity profiles, showing log-law with constants  $\kappa = 0.41$ ,  $A = 5.0$ .

(1.9) to the data. As the profiles evolve the wake strength decays, whilst the Kármán number (i.e.  $K_\tau = \delta_c U_\tau / \nu$ ) grows to its asymptotic value. Therefore the region of collapse with the log-law increases as the profiles evolve and by the most downstream stations the profiles are characterized by a log-law that extends almost to the edge of the layer.

An interesting feature of the Pitot-tube mean profiles is the slight ‘kick-up’ from the log-law which is observed near the buffer region. However this ‘kick-up’ region is not observed in velocity profiles measured with a normal hot wire. Figure 6(a) shows the discrepancy between hot-wire measurements and Pitot-tube measurements which have been corrected for shear using the MacMillan (1956) correction. The discrepancy suggests the Pitot-tube measurements may be suffering from turbulence effects, which is a consequence of the nonlinear relationship between pressure (or manometer output voltage) and the velocity. It has been shown by Jones (1998) that when the Pitot-tube is corrected for both turbulence effects and shear effects the agreement between the Pitot-tube profiles and normal-wire profiles is better and less ‘kick-up’ is observed, see figure 6(b). These results also confirm that the MacMillan

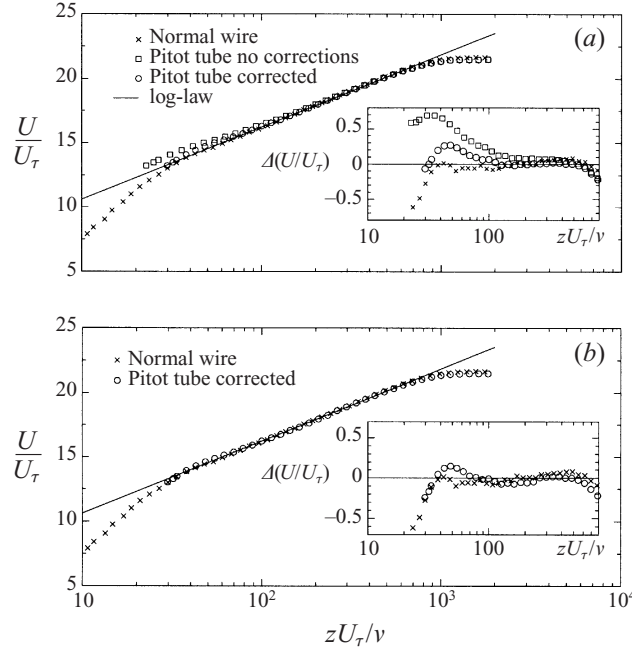


FIGURE 6. Mean velocity profile as measured with a normal hot wire, compared to (a) Pitot-static measurement with no corrections and MacMillan (1956) correction alone; (b) Pitot-static measurement with both MacMillan (1956) correction and turbulence correction. Insets show the deviation from the log-law, i.e.  $\Delta(U/U_\tau)$  with constants  $\kappa = 0.41$  and  $A = 5.0$ .

(1956) correction, which was developed for pipe flow, is valid, at least for the range of Reynolds numbers encountered here.

### 3.1. Wall shear velocity

It must be remembered that the Clauser chart was used to determine the values of  $U_\tau$ , which effectively forces the profiles to collapse onto the log-law with the specified constants. The validity of the Clauser chart values of  $U_\tau$  must therefore be examined. To facilitate this, use is made of the integral momentum equation. Unfortunately, in general, the direct use of (1.12) to determine  $C_f'$  is inaccurate since it involves differentiation of  $\theta$ . However once the flow achieves a state of equilibrium then  $R_\theta = \text{constant}$  in which case (1.12) becomes

$$KR_\theta(H + 1) = C_f'/2. \quad (3.1)$$

Using (3.1)  $U_\tau$  was calculated for station  $x = 3580$  mm and the results are compared to both the Clauser chart values and the Preston tube values (obtained using the Patel 1965 calibration) in table 1 and the agreement is found to be good. The good agreement suggests that a universal law of the wall (upon which both the Clauser chart and Preston tube methods are based) is valid, for the mild levels of acceleration encountered in this study. This is consistent with the original finding of Patel (1965), where the maximum error for a Preston tube was found to be  $< 3\%$  when exposed to a pressure gradient strength in the range  $0 < \Delta_p < -0.005$ , where  $\Delta_p$  is the pressure gradient parameter given by

$$\Delta_p = \frac{\nu}{\rho U_\tau^3} \frac{dp_1}{dx}. \quad (3.2)$$

| K                     | $\Delta_p$             | Momentum | Clauser chart |              | Preston tube |              |
|-----------------------|------------------------|----------|---------------|--------------|--------------|--------------|
|                       |                        | $U_\tau$ | $U_\tau$      | % $\epsilon$ | $U_\tau$     | % $\epsilon$ |
| $2.70 \times 10^{-7}$ | $-3.29 \times 10^{-3}$ | 1.3337   | 1.3289        | -0.4         | 1.3134       | -1.5         |
| $3.59 \times 10^{-7}$ | $-3.95 \times 10^{-3}$ | 0.9722   | 0.9932        | +2.2         | 0.9749       | +0.3         |
| $5.39 \times 10^{-7}$ | $-5.35 \times 10^{-3}$ | 0.6949   | 0.7010        | +0.9         | 0.6845       | -1.5         |

TABLE 1. Wall shear velocity  $U_\tau$  (m s<sup>-1</sup>) calculated from (3.1) compared with Clauser chart and Preston tube values, for station  $x = 3580$  mm and where % $\epsilon$  indicates the percentage difference.

For stations not in equilibrium, differentiation of  $\theta$  can be avoided by integrating (1.12) with respect to  $x$  between stations  $x_a$  and  $x$ . Following the approach of Coles (1956) the result of the integration can be expressed as

$$\frac{U_1^2 \theta}{U_{1a}^2 \theta_a} - 1 + \frac{1}{2} \int_1^{U_1^2/U_{1a}^2} \frac{\delta^*}{\theta_a} d \left( \frac{U_1^2}{U_{1a}^2} \right) = \phi(x) \quad (3.3)$$

where  $U_{1a} = U_1(x_a)$  and  $\theta_a = \theta(x_a)$  and the function  $\phi(x)$  in (3.3) is given by

$$\phi(x) = \int_{x_a}^x \frac{U_\tau}{\theta_a U_{1a}^2} dx. \quad (3.4)$$

For all flow cases  $\phi(x)$  was calculated using the two independent methods, given by (3.3) and (3.4). Sufficient conditions for these equations to agree are two-dimensional flow in the mean and correctly determined values of  $C_f'$ . It is possible that (3.3) and (3.4) would also balance if three-dimensional effects were exactly balanced by errors in  $C_f'$ , although this would appear highly improbable. When evaluating (3.4) both the Clauser chart and Preston tube values of  $U_\tau$  were used and the results are shown in figures 7(a) and 7(b) respectively. The agreement is very good, suggesting that the flow is two-dimensional in the mean and that the  $U_\tau$  values are accurate. The maximum difference between the curves given in figure 7(a) would be consistent with the Clauser chart overestimating  $U_\tau$  by approximately 1.5%. Whereas figure 7(b) suggests that the Preston tube may be slightly underestimating  $U_\tau$  and this is most noticeable at the highest level of acceleration ( $K = 5.39 \times 10^{-7}$ ) where the difference between the two curves would be indicative of an underestimation of approximately 2%.

#### 4. Evolution of mean flow parameters

The evolution of the mean flow parameters  $S$ ,  $\Pi$  and  $\delta_c$  is shown in figure 8, for each level of acceleration. Figure 9 shows the evolution of  $\beta$ .

The evolution of  $S$  is similar for the three acceleration parameters studied and it can be seen that for all cases  $S$  is initially increasing. However for streamwise coordinates  $x/L > 0.55$   $S$  appears to have reached a constant asymptotic value. This would be consistent with the boundary layer attaining a state of equilibrium, since as Rotta (1962) has shown  $S = \text{constant}$  is a required condition for precise equilibrium.

As the boundary layer evolves, the Coles wake strength factor  $\Pi$  decays. However only for the flow with the highest acceleration parameter ( $K = 5.39 \times 10^{-7}$ ) is 'pure wall' flow attained, as conjectured by Coles (1957). For the other flow cases  $\Pi$  shows a small but finite value at the most downstream station. However this does not necessarily contradict the pure wall hypothesis of Coles (1957) but may instead indicate that the layers have not quite reached the precise equilibrium state. It should

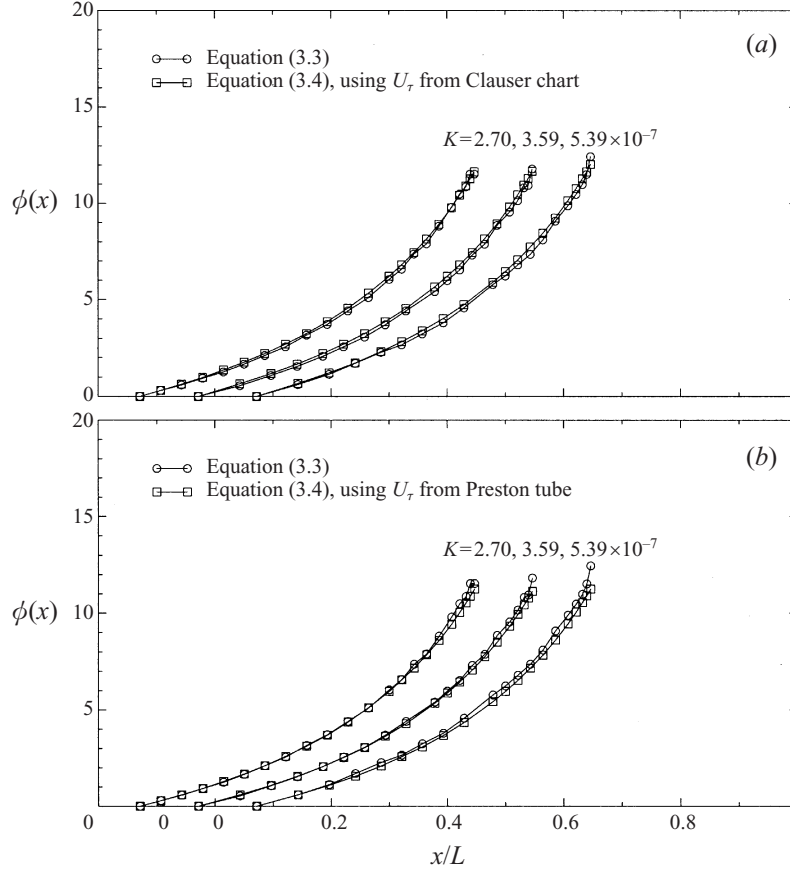


FIGURE 7. Momentum balance (a) using Clauser chart values for  $U_\tau$ . (b) Using Preston tube values for  $U_\tau$ .

be noted that there is difficulty involved in determining  $\Pi$  especially as  $\Pi \rightarrow 0$  and this is reflected in the scatter present in figure 8.

The boundary layer thickness  $\delta_c$  was determined such that the defect function obtained using (1.9) gave the required displacement thickness  $\delta^*$  as determined from experiment and therefore

$$\delta_c = \frac{\delta^* S}{C_1[\Pi]}. \quad (4.1)$$

For all flow cases the non-dimensional boundary layer thickness given by  $\delta_c U_0/\nu$  initially grows and reaches a maximum at around  $x/L = 0.4$ . Beyond this value the boundary layer thickness proceeds to diminish. For precise equilibrium, it is required that the gradient of the boundary layer thickness with respect to  $x$  becomes constant. However it is not clear from the data whether this condition has been reached, due to the experimental scatter inherent in  $d\delta_c/dx$ . Figure 10 shows a comparison with the length scale of Clauser (1954) which is given by

$$\Delta = \delta^* S. \quad (4.2)$$

This is preferred since estimating  $\Delta$  has less experimental error associated with it because the scatter in  $C_1[\Pi]$  has been removed for  $\Pi \rightarrow 0$ . As the virtual sink

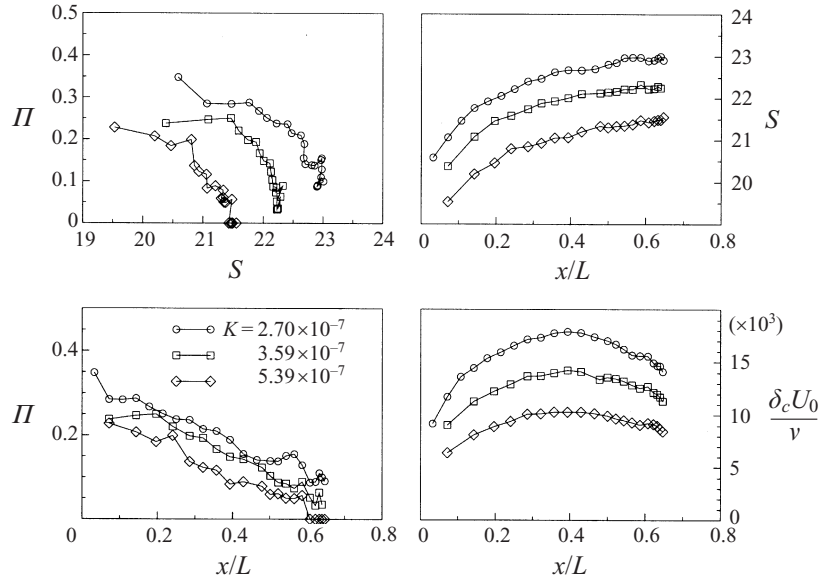
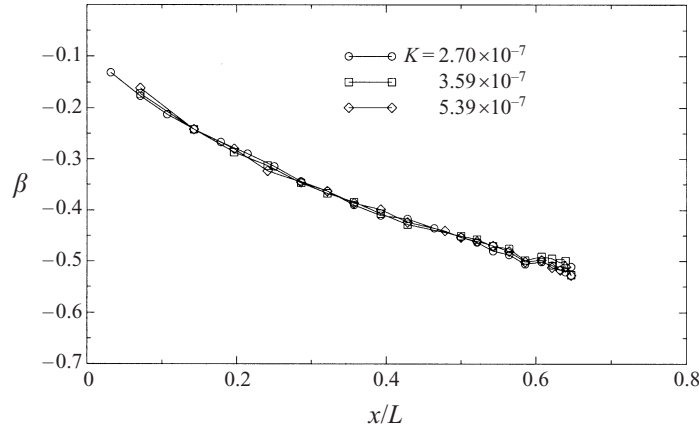


FIGURE 8. Evolution of mean flow parameters.

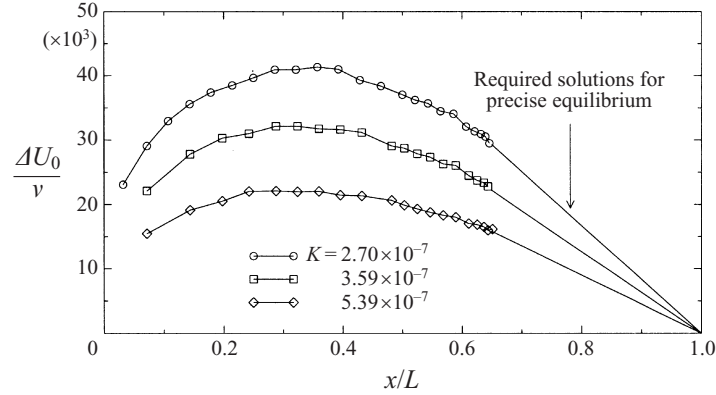
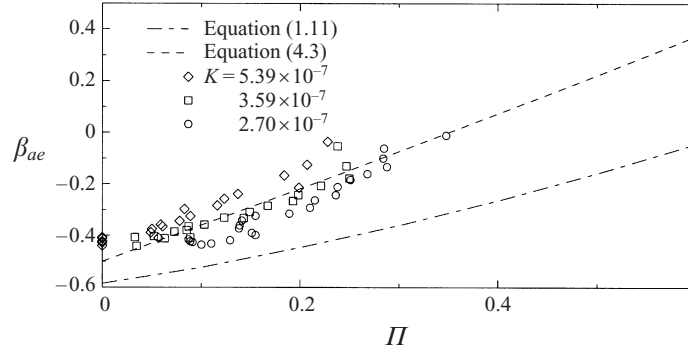
FIGURE 9. The evolution of  $\beta$  with non-dimensional streamwise coordinate  $x/L$ .

location is approached (i.e.  $x/L = 1.0$ ) it would be expected that all length scales tend to zero while all velocity scales approach infinity. This is required to ensure the local Reynolds number, no matter how constructed, remains constant and thus precise equilibrium is maintained. The data in figure 10, at stations  $x/L > 0.6$  appears to be consistent with this required gradient, but measurements further downstream would be required to draw a firmer conclusion.

#### 4.1. Comparison with predicted evolution

The experimental results of figure 8 are seen to agree only qualitatively with the predicted solutions of figure 2. In what follows, several reasons for the lack of quantitative agreement will be discussed.

The empirical input for the closure equation is the choice of  $\beta_{ac}[II]$  and the calculations given in figure 2 made use of the Green *et al.* (1973) function given

FIGURE 10. The evolution of  $\Delta$  with non-dimensional streamwise coordinate  $x/L$ .FIGURE 11. Experimental data for  $\beta_{ae}$  from current study along with curve fits.

by (1.11). However it was found that this function represents a poor choice: first it correlates data at finite  $S$  and secondly it is based on a data at values of  $\Pi$  higher than those encountered in this study. The experimental values of  $\beta$  for given experimental values of  $\Pi$  and  $S$  are mapped to infinite  $S$  using the matching technique given in (1.10). The results of this mapping process are given in figure 11 and it can be seen that (1.11) gives a poor fit to the experimental results. Jones (1998) proposes using the curve fit

$$\beta_{ae} = -0.5 + 1.38\Pi + 0.13\Pi^2, \quad (4.3)$$

which correlates the low- $\Pi$  data better as well as fitting approximate equilibrium data at higher  $\Pi$  values. However it should be noted that while (4.3) gives a better general fit to the data, the data do exhibit a high degree of scatter which may indicate that although  $\zeta$  does not play a strong part in the momentum balance it seems to have an appreciable effect on the asymptotic form for  $\beta$ . It is interesting to note that for precise equilibrium, i.e.  $dS/dR_x = 0$ , (1.13) gives

$$\beta = \frac{-C_1[\Pi]S}{2C_1[\Pi]S - C_2[\Pi]} \quad (4.4)$$

and for  $S \rightarrow \infty$  (4.4) then gives  $\beta_{ae} = -1/2$ . Assuming  $\Pi \rightarrow 0$ , (4.3) is consistent with this result.

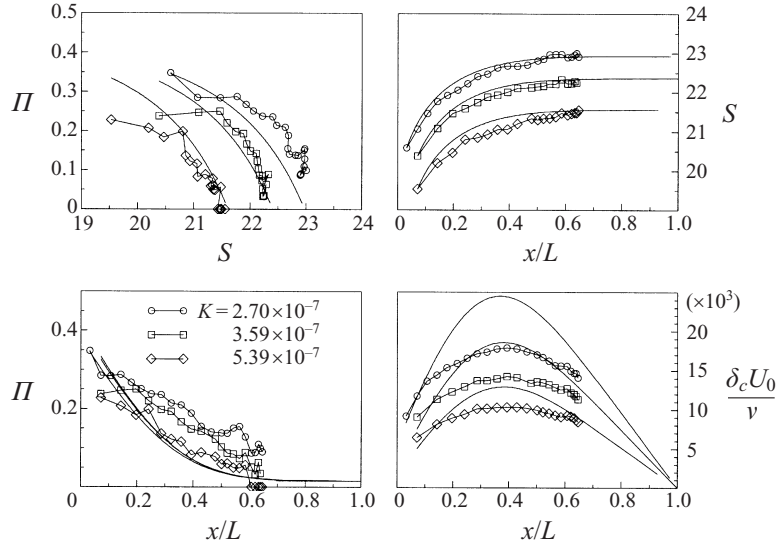


FIGURE 12. Solution to evolution equations using new formulation for  $\beta_{ae}$  (see equation (4.3)), compared with data.

Using (4.3) in the closure equation (1.10) and with auxiliary equation (1.14) evolution equation (1.13) was solved for the three levels of acceleration encountered and the results are compared in figure 12. Note that for these calculations the evolution equations are solved starting from the initial measured profile rather than the trip wire. Here the comparison is better than the predictions given in figure 2. Nevertheless it appears that the parameter  $\zeta_a$  must be included when determining the asymptotic behaviour of  $\beta$ , where  $\zeta_a$  is the asymptotic value of  $\zeta$ . That is, we must consider  $\beta_a[\Pi, \zeta_a]$ , where  $\beta_a$  denotes the asymptotic behaviour of  $\beta$  for general non-equilibrium flows; hence the subscript  $e$  has been dropped. Incorporating the inclusion of the  $\zeta$  parameter is considered in a paper currently under preparation.

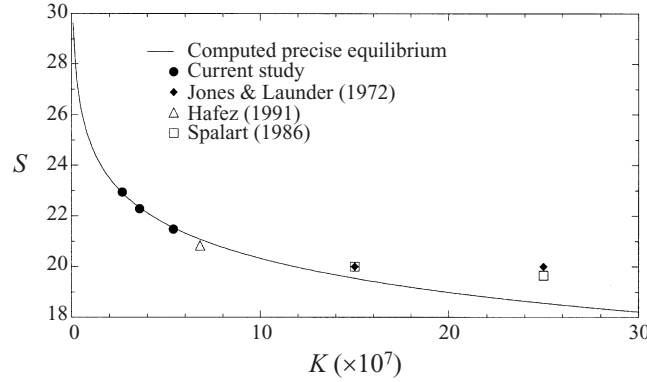
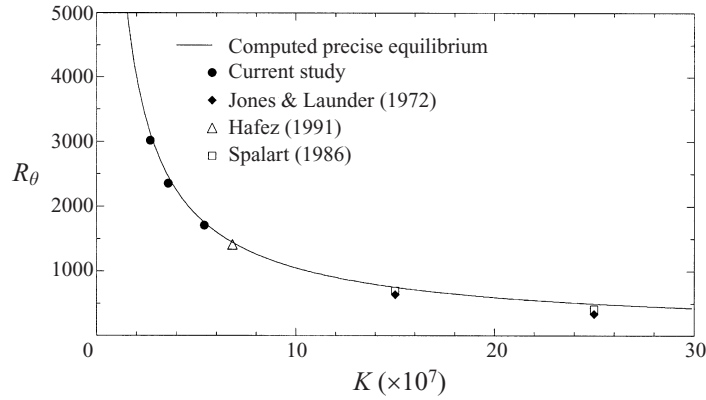
#### 4.2. Asymptotic solution

To investigate whether the boundary layers have reached a state of precise equilibrium, the experimental results are compared to the predicted precise equilibrium solutions. Making use of (1.9) expressions for  $R_\theta$  and  $H$  can be generated in terms of the mean flow parameters  $S$  and  $\Pi$  alone which when substituted into (3.1) give

$$S^2 E[\Pi] \exp[\kappa S] C_1[\Pi] K (-2SC_1[\Pi] + C_2[\Pi]) + SC_1[\Pi] = 0. \quad (4.5)$$

Using the hypothesis of Coles (1957) that  $\Pi = 0$  for an equilibrium sink flow, the asymptotic solution for  $S$  as a function of  $K$  was determined from (4.5) and the result is shown in figure 13. The average experimental value of  $S$  (beyond station  $x/L = 0.58$ ) is also plotted in figure 13 and it shows excellent agreement with the predicted equilibrium solution.

The asymptotic values of  $S$  for the studies of Jones & Launder (1972) and Spalart (1986) are also shown in figure 13 and their results do not agree with the current prediction. However it should be kept in mind that the data at  $K = 2.5 \times 10^{-6}$  correspond to a low Reynolds number boundary layer ( $R_\theta \approx 400$ ) so that describing the mean profile by the logarithmic law of the wall and law of the wake alone is not

FIGURE 13. Precise equilibrium solution for  $S$  as a function of  $K$ , solution from (4.5).FIGURE 14. Precise equilibrium solution for  $R_\theta$  as a function of  $K$ , solution using (4.5) and (4.6).

longer sufficiently accurate and inclusion of a buffer zone and sublayer is needed when generating expressions for the required mean profile parameters. Actually a review on the subject of relaminarization by Narasimha & Sreenivasan (1979) suggests that the turbulent flow cannot be maintained for  $K$  values greater than about  $2.5 \times 10^{-6}$  to  $3.0 \times 10^{-6}$ . Even for  $K$  values greater than about  $1.0 \times 10^{-6}$  the mean profile shows no discernible log law region (see Jones & Launder 1972).

Once  $S$  versus  $K$  has been found, all other asymptotic mean flow parameters can be found using the log-law of the wall and law of the wake, for example  $R_\theta$  which is given by

$$R_\theta = S \exp[\kappa S] E[\Pi] \left( \frac{C_1[\Pi]}{S} - \frac{C_2[\Pi]}{S^2} \right). \quad (4.6)$$

Using the solution from (4.5) and again assuming pure wall flow (i.e.  $\Pi = 0$ ) (4.6) can be solved to give the predicted equilibrium solution for  $R_\theta$  as a function of  $K$  and it is shown in figure 14, along with the experimental average value beyond station  $x/L = 0.58$ . Again for the data of the current study agreement with the predicted equilibrium solution is very good, suggesting the flows are close to precise equilibrium at the most downstream stations.



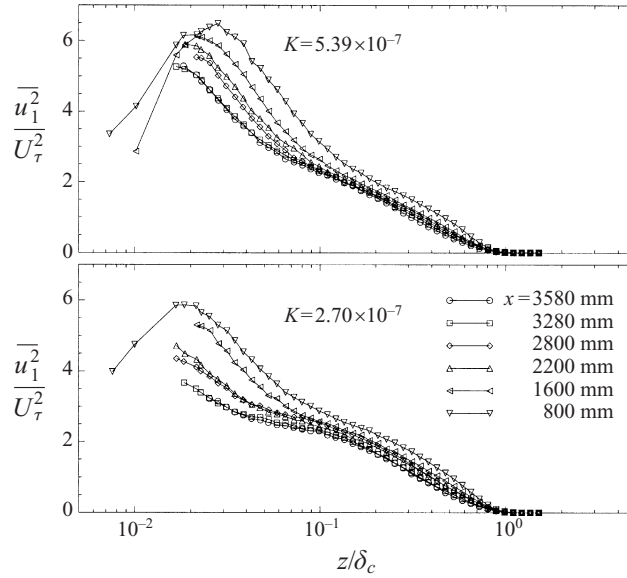


FIGURE 15. Evolution of streamwise turbulence intensities.

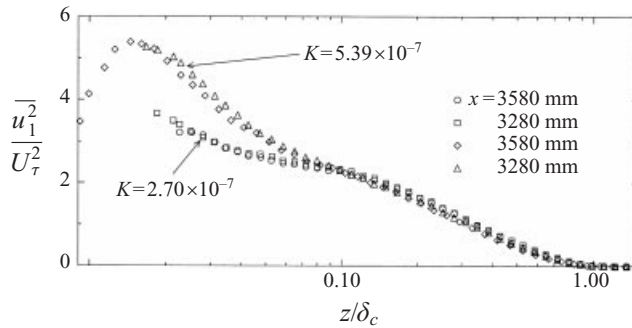


FIGURE 16. Similarity profiles of streamwise turbulence intensities, using outer flow scaling.

## 5. Reynolds stresses

Reynolds stress measurements were taken for flows  $K = 2.70 \times 10^{-7}$  and  $K = 5.39 \times 10^{-7}$  at the streamwise stations  $x = 800, 1600, 2200, 2800, 3280$  and  $3580$  mm.

### 5.1. Streamwise turbulence intensities

The evolution of the streamwise turbulence intensities is shown in figure 15. For each value of  $K$ , the  $\overline{u_1^2}/U_\tau^2$  profile shape is seen to become invariant with streamwise distance for  $x > 3280$  mm. This is shown more clearly in figure 16 and it can also be seen that in the region  $z/\delta_c > 0.08$  the profiles for different values of  $K$  (i.e. Reynolds number) show collapse. Further the profiles in this region are closely described by a logarithmic profile. Once precise equilibrium is reached all local Reynolds numbers become invariant with  $x$  and for stations  $x > 3280$  mm both  $K_\tau$  and  $R_\theta$  appear to be asymptoting to constant values which are consistent with predictions (e.g. see figure 14). Hence if the equilibrium profiles are plotted using inner flow scaling, similarity should also exist for a given value of  $K$  and this is shown in figure 17. Here a comparison is also made with the sink-flow simulation of Spalart (1986). The

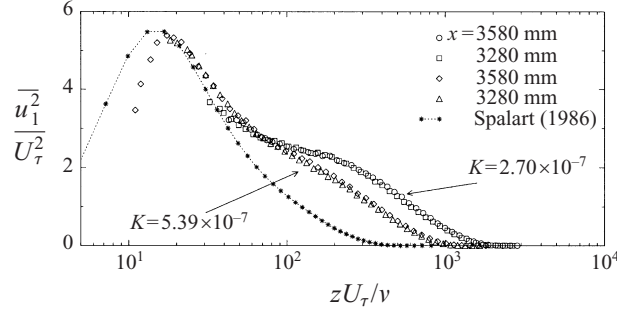


FIGURE 17. Similarity profiles of streamwise turbulence intensities, using inner flow scaling. Also shown is the simulation of Spalart (1986) for a sink flow with  $K = 1.5 \times 10^{-6}$  ( $R_\theta = 690$  and  $K_\tau \approx 550$ ).

interesting feature is that the location and value of the maximum stress for the profile of Spalart (1986) is very close to the experimental value, for the profile where it was obtainable.

The existence of a region where  $\overline{u_1^2}$  is described by a logarithmic function was first suggested by Townsend (1976). Using the attached eddy hypothesis Townsend (1976) showed that a logarithmic relationship would exist for the region  $\delta_1 \ll z \ll \delta_2$ , where  $\delta_1$  and  $\delta_2$  are the length scales of the smallest and largest eddies respectively and this condition essentially requires a sufficiently high Reynolds number layer.

Using the attached eddy model proposed by Perry & Chong (1982) in conjunction with a dimensional argument, Perry, Henbest & Chong (1982) proposed spectral scaling laws and turbulence intensity scaling laws applicable to the fully turbulent wall region. The fully turbulent wall region is defined as the region where the mean velocity profiles collapse onto the standard logarithmic law and in addition  $z \ll \delta_c$ , and here the limits proposed by Perry, Lim & Henbest (1987), of  $z_+ \geq 100$  and  $z/\delta_c < 0.15$  for zero pressure gradient layers are adopted. Note that  $z_+ = zU_\tau/\nu$ . The results of Perry *et al.* (1986) were further refined by Perry & Li (1990) leading to a scaling law for the streamwise turbulence intensity given by

$$\frac{\overline{u_1^2}}{U_\tau^2} = B_1 - A_1 \ln \left[ \frac{z}{\delta_c} \right] - V[z_+]. \quad (5.1)$$

Here  $A_1$  is a universal constant while  $B_1$  is a large-scale characteristic constant and the last term is the viscous correction term. From spectral data for the zero pressure gradient layer Perry *et al.* (1987) find  $A_1 = 1.03$ . In fact this value agrees very well with the  $\overline{u_1^2}/U_\tau^2$  log-law distributions in the more recent work of Marusic, Uddin & Perry (1997) for  $K_\tau$  from  $2.5 \times 10^3$  to  $2.3 \times 10^4$  or  $R_\theta$  from  $6 \times 10^3$  to  $6 \times 10^4$  (see Marusic *et al.* 1997, figure 6).

The function  $V[z_+]$  is the viscous correction term, which was numerically computed by Perry & Li (1990), assuming a zero pressure gradient layer and S. H. M. Hafez (private communication) found their result could be described by the function

$$V[z_+] = 5.58(1 - z_+^{-0.9})z_+^{-1/2}. \quad (5.2)$$

Further Hafez (1991) found that by fitting limited streamwise turbulence data to (5.1) and in conjunction with (5.2),  $B_1$  can be correlated with  $\Pi_c$  and suggests the relation

$$B_1[\Pi_c] = 0.41 + 3.7\Pi_c - 0.76\Pi_c^2; \quad (5.3)$$

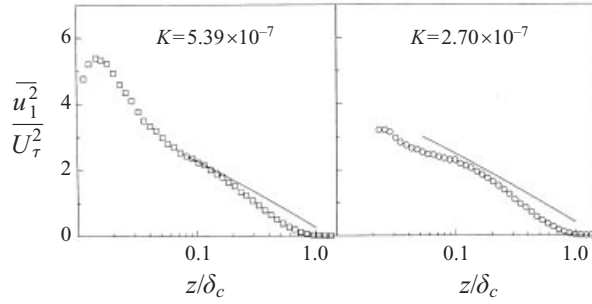


FIGURE 18. Streamwise turbulence intensities with fit of equation (5.1) given by the solid line for  $z_+ > 100$ , for station 3580 mm.

here  $\Pi_c$  is the Coles wake factor using the traditional Coles (1956) log-law of the wall and law of the wake, i.e. the corner function is not included when fitting (1.9) to data (see Appendix C for the relation between  $\Pi$  and  $\Pi_c$ ). Figure 18 shows the fit of (5.1) using  $A_1 = 1.03$ , (5.2) and (5.3), for both flow cases, at the most downstream station (i.e.  $x = 3580$  mm). For the low Reynolds number case ( $K = 5.39 \times 10^{-7}$ ,  $K_\tau = 1200$ ) the length of the fully turbulent wall region is relatively small, nevertheless (5.1) does give a fairly good fit in this region. However for the higher Reynolds number case ( $K = 2.70 \times 10^{-7}$ ,  $K_\tau = 1891$ ) the fit of (5.1) is poor. The deviation from (5.1) is most pronounced as the lower bound of the fully turbulent wall region is approached, i.e.  $z_+ \rightarrow 100$  and this suggests the functional form of  $V[z_+]$  as given by (5.2) may not be correct. When deriving  $V[z_+]$  Perry & Li (1990) assume that in the fully turbulent wall region

$$-\overline{u_1 u_3} \approx U_\tau^2 \quad (5.4)$$

and further that dissipation equals production and this allows the Kolmogorov length and velocity scales to be expressed in terms of wall variables. The assumptions outlined above are true for the zero pressure gradient layer. However for the sink flows of the current study the fully turbulent wall region does not correspond to a region of constant Reynolds shear stress and thus (5.4) is not a valid assumption unless  $z/\delta_c$  is extremely small and the Reynolds number is sufficiently high.

### 5.2. Spanwise and normal turbulence intensities

The spanwise turbulence intensities are shown in figure 19 and for a given value of  $K$  the profiles evolve to a self-similar state by the last two stations, where they are characterized by a semi-logarithmic profile. In figure 20 the similarity profiles for different values of  $K$  are compared and they are found to collapse beyond  $z/\delta_c \approx 0.15$ .

Based on the spectral scaling arguments of Perry *et al.* (1986) the expected spanwise turbulence intensity in the fully turbulent wall region is given by Perry & Li (1990) as

$$\frac{\overline{u_2^2}}{U_\tau^2} = B_2 - A_2 \ln \left[ \frac{z}{\delta_c} \right] - V[z_+], \quad (5.5)$$

where  $B_2$  is a characteristic large-scale constant and  $A_2$  is a universal constant. From spectral data Perry & Li (1990) propose that  $A_2 = 0.475$ ; further since  $V[z_+]$  is isotropic they also propose it will take the form given in (5.2). It was found by Jones (1998) that (5.5) using  $A_2 = 0.475$  and (5.2) generally gave a poor fit to data in the fully turbulent wall region. Again it is suggested that  $V[z_+]$  as given in (5.2) is not appropriate for the sink flows considered here.

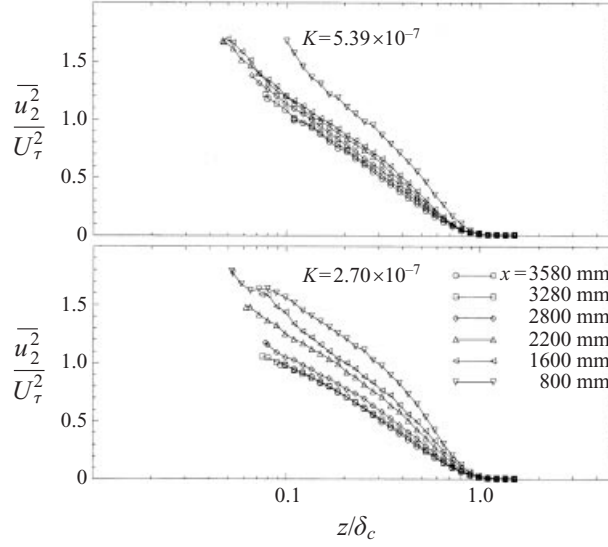


FIGURE 19. Evolution of spanwise turbulence intensities.

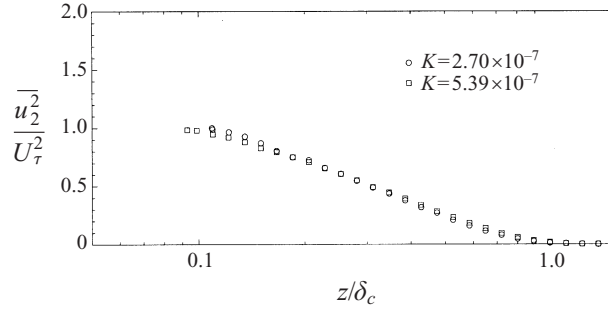


FIGURE 20. Similarity profiles of spanwise turbulence intensities.

The behaviour of the normal turbulence intensity is very similar to that for the spanwise turbulence intensity and is shown in figure 21 for completeness. For both values of  $K$  the profiles evolve to the same self-similar profile, which is well described by a logarithmic profile. Such a logarithmic profile is not predicted by the fully turbulent wall-region scaling laws; in fact Perry & Li (1990) propose the scaling law

$$\frac{\overline{u_3^2}}{U_\tau^2} = A_3 - V[z_+] \quad (5.6)$$

in the fully turbulent wall region. However, it is expected that (5.6) would be valid for  $z/\delta_c < 0.1$  and  $z_+ > 100$  but unfortunately, as the Reynolds shear stress profiles show, there is likely to be a problem with X-wires in this region.

### 5.3. Reynolds shear stress

The Reynolds shear stress profiles are shown in figure 22 and their development follows the same trends for both values of  $K$ . As the layers develop the profiles become less full, evolving to a self-similar state at stations  $x = 3280$  and  $x = 3580$  mm. The expression for the total shear stress, given in (1.5), is found to be in reasonable agreement with the Reynolds shear stress measurements. By subtracting the viscous

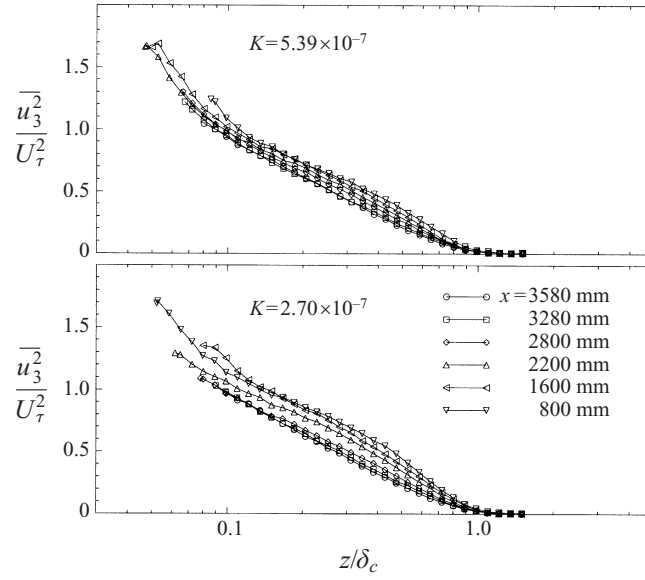
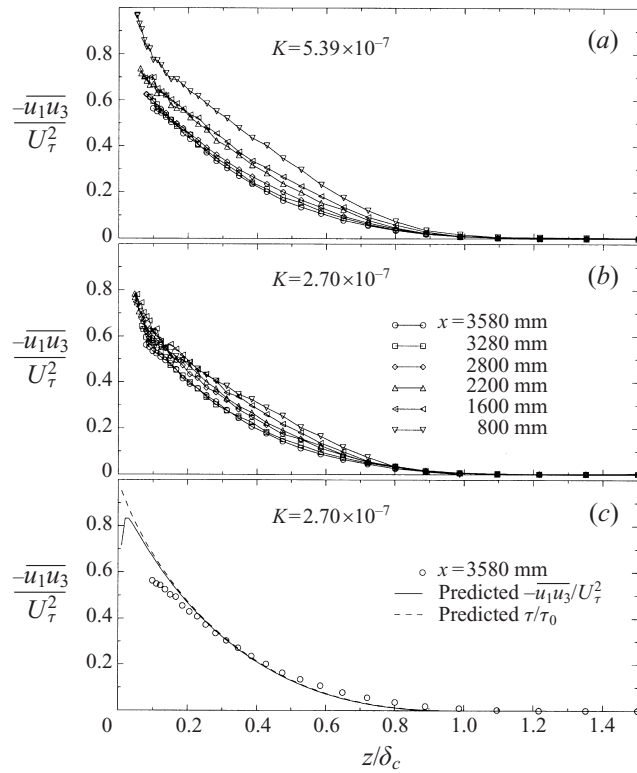


FIGURE 21. Evolution of normal turbulence intensities.

FIGURE 22. Reynolds shear stress profiles: (a)  $K = 5.39 \times 10^{-7}$ , (b)  $K = 2.70 \times 10^{-7}$  and (c) example comparison with predicted Reynolds shear stress.

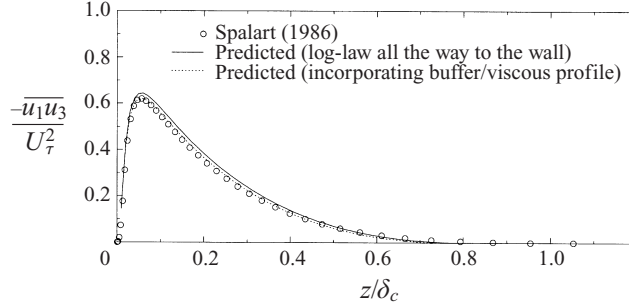


FIGURE 23. Predicted Reynolds shear stress profile compared with the simulation of Spalart (1986) for a sink flow with  $K = 1.5 \times 10^{-6}$  ( $R_\theta = 690$  and  $K_\tau \approx 550$ ).

contribution from the total shear stress, predictions for the Reynolds shear stress are then given by

$$\frac{-\overline{u_1 u_3}}{U_\tau^2} = \frac{\tau}{\tau_0} - \frac{d(U/U_\tau)}{d(zU_\tau/\nu)}, \quad (5.7)$$

where  $\tau/\tau_0$  is given by (1.5) and the viscous contribution is calculated using the Reichardt (1951) mean velocity profile as given in Appendix B. A typical comparison between the predicted Reynolds shear stress and data is shown in figure 22. The agreement is seen to be quite good except that the measured stress is generally lower than the prediction close to the wall but is higher in the outer part of the layer. The results of Jones & Launder (1972) also show a similar trend when compared to the prediction, although the magnitude of their discrepancies is much greater. On the other hand when the results of the Spalart (1986) simulation are compared with the predicted Reynolds shear stress profile the agreement is better. In figure 23 the profile of Spalart (1986) is compared to the predicted Reynolds shear stress derived assuming the log-law goes all the way to the wall (i.e. using (1.5) in conjunction with (5.7)) and it is also compared to the Reynolds shear stress when a viscous/buffer profile is used close to the wall when deriving (1.5). The results of Spalart (1986) tend to support the validity of (1.5) and this suggests that the X-wire measurements may have higher errors than usual. This may be due to the very high shear experienced across the X-wire in this flow. At the present time, the authors are not aware of any existing feasible correction scheme which could be applied. It is also worth noting that the difference between the predicted curves in figure 23 indicates that the total shear stress expression given by (1.5) should be accurate down to Kármán numbers of  $K_\tau \approx 600$ .

## 6. Spectra in the fully turbulent wall region

Spectra measurements were made at four stations:  $x = 1600$ ,  $x = 2200$ ,  $x = 2800$  and  $x = 3280$  mm for acceleration parameters  $K = 5.39 \times 10^{-7}$  and  $K = 2.70 \times 10^{-7}$ . Both normal wires and X-wires were used to obtain spectra measurements for all three velocity components.

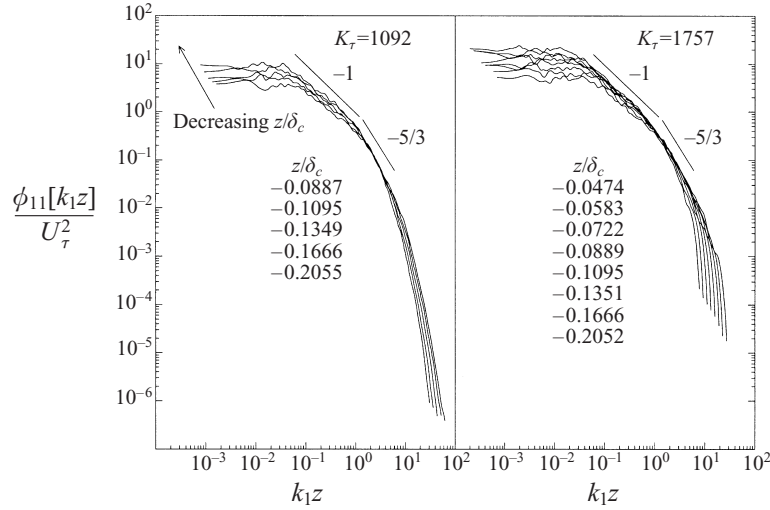
In the following the power spectral density  $\phi_{ij}[k_1 l]$  is defined as the spectrum per unit non-dimensional wavenumber  $k_1 l$ , that is

$$\phi_{ij}[k_1 l] = \frac{\phi_{ij}[k_1]}{l} \quad (6.1)$$

where  $k_1$  is the wavenumber and  $l$  is some length scale.

| $K$                   | $R_\theta$ | $K_\tau$ | $\Pi$ | $S$    |
|-----------------------|------------|----------|-------|--------|
| $5.39 \times 10^{-7}$ | 1670       | 1092     | 0.06  | 21.478 |
| $2.70 \times 10^{-7}$ | 2946       | 1757     | 0.12  | 22.978 |

TABLE 2. Mean flow parameters for station 3280 mm.

FIGURE 24. Streamwise spectra in the fully turbulent wall region, with wall-variable scaling, station  $x = 3280$  mm.

Here attention will be focused on the streamwise spectra results in the fully turbulent wall region for the most downstream station since these results represent approximately pure wall flow, at two different Reynolds numbers, and table 2 summarizes the mean flow parameters at this station. From the values of  $\Pi$  given in table 2 it can be seen that the lower Reynolds number results more closely approximate pure wall flow.

Making use of the attached eddy hypothesis in conjunction with dimensional analysis Perry *et al.* (1986) proposed that the streamwise spectra in the fully turbulent wall region will collapse for moderate to high wavenumber motions, when scaled with inner-flow variables  $z$  and  $U_\tau$  as opposed to outer flow variables  $\delta_c$  and  $U_\tau$ . Using an overlap region argument they show that the spectra in the region of collapse will be described by two universal power laws: for moderate wavenumbers

$$\frac{\phi_{11}[k_1 z]}{U_\tau^2} = \frac{A_1}{k_1 z} \quad (6.2)$$

and for higher wavenumbers

$$\frac{\phi_{11}[k_1 z]}{U_\tau^2} = \frac{1}{\kappa^{2/3}} \frac{K_0}{(k_1 z)^{5/3}}, \quad (6.3)$$

where  $K_0$  is the universal Kolmogorov constant. It should be noted that when deriving the form of (6.3) Perry *et al.* (1986) assume  $-\overline{u_1 u_3} \approx U_\tau^2$  in the fully turbulent wall region and this is nominally true for the zero pressure gradient layer. However for the current results a constant Reynolds shear stress does not exist in the fully turbulent

wall region and thus (6.3) would not necessarily be anticipated, whereas the form of (6.2) does not rely on  $-\overline{u_1 u_3} \approx U_\tau^2$  and therefore should be valid for the current results. However the streamwise spectra results show very limited regions of collapse, see figure 24. For the lower Kármán number results little if any region of collapse exists and certainly no  $-1$  power law is apparent. The higher Kármán number results do show a small region of collapse, however the short region does not allow any convincing conclusions to be made concerning the existence of a  $-1$  power law. The current results do not necessarily imply that the  $-1$  power law will not exist for sink flows. It may be that the definition of the fully turbulent wall region is too liberal and to satisfy the condition  $z/\delta_c \ll 1.0$  while  $z_+ > 100$  requires much higher Kármán numbers, that is a larger separation between the smallest and largest eddies. This observation is also supported by the attached eddy model predictions of Perry & Marusic (1995) and Marusic & Perry (1995).

The spanwise and normal spectra also lack any convincing power laws as predicted by Perry *et al.* (1986). Again it is believed this is due to the relatively low Kármán numbers of the flows being considered.

## 7. Conclusions and discussion

Using the experimental results a new formulation describing the asymptotic behaviour of  $\beta$  for approximate equilibrium layers is proposed (i.e.  $\beta_{ae}$ ). When this function is incorporated in the closure hypothesis of Perry *et al.* (1994) the solutions for the boundary layer evolution are found to give reasonably good agreement with the experimentally observed evolution. Nevertheless it appears that for the cases studied here the parameter  $\zeta$  may have to be considered for the calculations to more accurately predict the evolution.

The state of the layers by the most downstream stations agrees well with the predicted precise equilibrium solutions obtained using the integral momentum equation. Also the mean profiles and Reynolds stress profiles, for a given flow case, were found to reach a self-similar state by the most downstream stations. These observations therefore suggest that the boundary layers attained a state very close to the a precise equilibrium. Further the structure of the layers at the equilibrium stations was close to pure wall flow, that is a low wake factor  $\Pi$ . However it is difficult to say from experimental data whether a precise equilibrium sink flow corresponds exactly to pure wall flow, i.e.  $\Pi = 0$  at finite  $S$ . Calculations indicate that  $\Pi$  approaches a small but positive value at finite  $S$  and  $\beta$  is slightly more negative than  $-1/2$  as is indicated by (4.4).

The mean velocity profiles are characterized by a log-law that extends almost to the edge of the layer and the log-law constants were consistent with the conventional values of  $\kappa = 0.41$  and  $A = 5.0$ .

There was little evidence of the  $-1$  and  $-5/3$  power laws expected when considering the spectra in the fully turbulent wall region and it is felt this is due to the relatively low Reynolds numbers of the layers. Hence, while the mean profile shows a long log-law this is not sufficient to ensure a fully turbulent wall region. However the streamwise and spanwise Reynolds stress profiles did exhibit logarithmic behaviour as predicted by the fully turbulent wall-region scaling laws but this may have been fortuitous for these low Reynolds numbers.

The authors wish to acknowledge the financial assistance of the Australian Research Council.



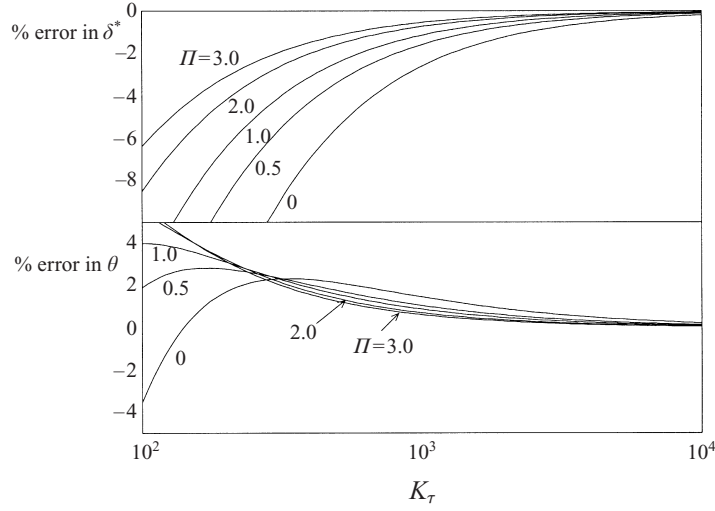


FIGURE 25. Effect of low Reynolds number (i.e. Kármán number) when evaluating the displacement and momentum thickness, assuming the logarithmic law is valid all the way to the wall compared to assuming (B 3) close to the wall.

### Appendix A. Functional forms

$$E[\Pi] = \exp \left[ -\kappa \left( A + \frac{2\Pi}{\kappa} - \frac{1}{3\kappa} \right) \right], \quad (\text{A } 1)$$

$$R[S, \Pi, \beta] = \frac{2C_1\beta S + C_1S - \beta C_2}{C_1(\kappa C_1 S^2 - C_2\kappa S + C_2)}, \quad (\text{A } 2)$$

where

$$C_1[\Pi] = \int_0^1 \frac{U_1 - U}{U_\tau} d\eta = (\Pi + (3/4))/\kappa, \quad (\text{A } 3)$$

$$C_2[\Pi] = \int_0^1 \left( \frac{U_1 - U}{U_\tau} \right)^2 d\eta = (1248\Pi^2 + 2140\Pi + 1215)/(840\kappa^2). \quad (\text{A } 4)$$

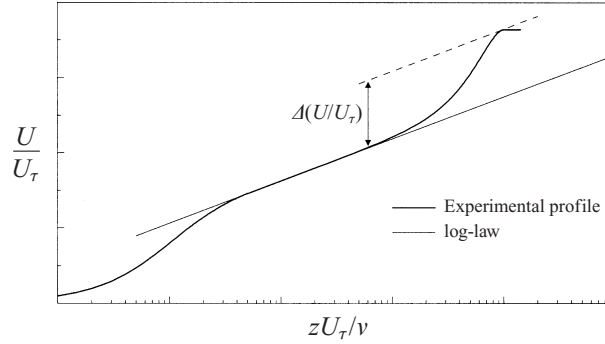
### Appendix B. Errors in $\delta^*$ and $\theta$ for low Reynolds numbers

Expressions for the displacement thickness and momentum thickness are

$$\frac{\delta^*}{S} = \frac{1}{S} \int_0^1 \frac{U_1 - U}{U_\tau} d\eta \quad (\text{B } 1)$$

$$\frac{\theta}{S} = \frac{1}{S} \int_0^1 \frac{U_1 - U}{U_\tau} d\eta - \frac{1}{S^2} \int_0^1 \left( \frac{U_1 - U}{U_\tau} \right)^2 d\eta. \quad (\text{B } 2)$$

For sufficiently high Reynolds numbers the contribution of the viscous and buffer regions to the integrals appearing in the above is negligible and (1.9) can be assumed valid all the way to the wall, in which case the integrals are universal functions of  $\Pi$  alone as given in (A 3) and (A 4). However for low Reynolds numbers the viscous and buffer regions must be included when evaluating the integrals which gives  $C_1[\Pi, K_\tau]$  and  $C_2[\Pi, K_\tau]$ . Figure 25 shows the error introduced in  $\delta^*$  and  $\theta$  as a function of

FIGURE 26. Method for determining  $\Pi$ .

the Kármán number for different values of  $\Pi$ . In order to calculate  $C_1$  and  $C_2$  when the viscous and buffer regions are included the Reichardt (1951) profile was used to describe the law of the wall and it is given by

$$\frac{U}{U_\tau} = \frac{1}{\kappa} \ln [1 + \kappa z^+] + \left( A - \frac{\ln [\kappa]}{\kappa} \right) \left( 1 - \exp \left[ \frac{-z^+}{11} \right] - \frac{z^+}{11} \exp [-0.33z^+] \right). \quad (\text{B } 3)$$

### Appendix C. The Coles wake factor

To determine  $\Pi$  the maximum deviation from the logarithmic law is determined and is denoted by  $\Delta(U/U_\tau)$ , see figure 26. Using a Coles traditional log-law of the wall and law of the wake formulation (i.e. the corner function is omitted from (1.9)) it can be shown that

$$\Delta \left( \frac{U}{U_\tau} \right) = \frac{2\Pi_c}{\kappa}. \quad (\text{C } 1)$$

However when the corner function is included it can be shown from (1.9) that

$$\Delta \left( \frac{U}{U_\tau} \right) = \frac{288\Pi^3}{\kappa(12\Pi + 1)^2}. \quad (\text{C } 2)$$

The above equations therefore give the relationship between traditional values of the Coles wake factor (i.e.  $\Pi_c$ ) and those quoted in this paper (i.e.  $\Pi$ ).

### REFERENCES

- CLAUSER, F. H. 1954 Turbulent boundary layers in adverse pressure gradients. *J. Aero. Sci.* **21**, 91–108.
- CLAUSER, F. H. 1956 The turbulent boundary layer. *Adv. Mech.* **4**, 1–51.
- COLES, D. E. 1956 The law of the wake in the turbulent boundary layer. *J. Fluid Mech.* **1**, 191–226.
- COLES, D. E. 1957 Remarks on the equilibrium turbulent boundary layer. *J. Aero. Sci.* **24**, 459–506.
- ERM, L. P. & JOUBERT, P. N. 1991 Low Reynolds number turbulent boundary layers. *J. Fluid Mech.* **230**, 1–44.
- GREEN, J. E., WEEKS, D. J. & BROOMAN, J. W. F. 1973 Prediction of turbulent boundary layers and wakes in compressible flow by a lag-entrainment method. *Aero. Res. Council. R and M* 3791.
- HAFEZ, S. H. M. 1991 The structure of accelerated turbulent boundary layers. PhD thesis, University of Melbourne, Australia.
- HERRING, H. J. & NORBURY, J. F. 1967 Experiments on equilibrium turbulent boundary layers in favourable pressure gradients. *J. Fluid Mech.* **27**, 541–549.

- JONES, M. B. 1998 Evolution and structure of sink-flow turbulent boundary layers. PhD thesis, University of Melbourne, Australia.
- JONES, W. P. & LAUNDER, B. E. 1972 Some properties of sink flow turbulent boundary layers. *J. Fluid Mech.* **56**, 337–351.
- LEWKOWICZ, A. K. 1982 An improved universal wake function for turbulent boundary layers and some of its consequences. *Z. Flugwiss. Weltraumforsch.* **6**, 261–266.
- MACMILLAN, F. 1956 Experiments on pitot-tubes in shear flow. *Aero. Res. Council. R & M* 3028.
- MARUSIC, I. & PERRY, A. E. 1995 A wall-wake model for the turbulence structure of boundary layers, part 2. Further experimental support. *J. Fluid Mech.* **298**, 389–407.
- MARUSIC, I., UDDIN, A. K. M. & PERRY, A. E. 1997 Similarity law for the streamwise turbulence intensity in zero-pressure-gradient turbulent boundary layers. *Phys. Fluids* **9**, 3718–3726.
- MOSES, H. L. 1964 The behavior of turbulent boundary layers in adverse pressure gradients. *Rep. 73*. Gas Turbine Lab., Mass. Inst. Techn.
- NARASIMHA, R. & SREENIVASAN, K. R. 1979 Relaminarization of fluid flows. *Adv. Appl. Mech.* **19**, 221–309.
- PATEL, V. 1965 Calibration of the preston tube and limitations on its use in pressure gradients. *J. Fluid Mech.* **23**, 185–205.
- PERRY, A. E. 1982 *Hot-wire Anemometry*. Clarendon.
- PERRY, A. E. & CHONG, M. S. 1982 On the mechanism of wall turbulence. *J. Fluid Mech.* **119**, 173–217.
- PERRY, A. E., HENBEST, S. M. & CHONG, M. S. 1986 A theoretical and experimental study of wall turbulence. *J. Fluid Mech.* **165**, 163–199.
- PERRY, A. E. & LI, J. D. 1990 Experimental support for the attached eddy hypothesis in zero-pressure-gradient turbulent boundary layers. *J. Fluid Mech.* **218**, 405–438.
- PERRY, A. E., LIM, K. L. & HENBEST, S. M. 1987 An experimental study of the turbulence structure in smooth- and rough-wall boundary layers. *J. Fluid Mech.* **177**, 437–466.
- PERRY, A. E. & MARUSIC, I. 1995 A wall-wake model for the turbulence structure of boundary layers, part 1. Extension of the attached eddy hypothesis. *J. Fluid Mech.* **298**, 361–388.
- PERRY, A. E., MARUSIC, I. & LI, J. D. 1994 Wall turbulence closure based on classical similarity laws and the attached eddy hypothesis. *Phys. Fluids* **6**, 1024–1035.
- PERRY, A. E. & MORRISON, G. L. 1971a A study of the constant temperature hot-wire anemometer. *J. Fluid Mech.* **47**, 577–599.
- PERRY, A. E. & MORRISON, G. L. 1971b Static and dynamic calibrations of constant temperature hot-wire systems. *J. Fluid Mech.* **47**, 765–777.
- REICHARDT, H. 1951 Volständige darstellung der turbulenten geschwindigkeitsverteilung in glatten leitungen. *Ze. Angew. Math. Mech.* **31**, 208.
- ROTTA, J. C. 1962 Turbulent boundary layers in incompressible flow. *Prog. Aero. Sci.* **2**, 1–219.
- SPALART, P. R. 1986 Numerical study of sink-flow boundary layers. *J. Fluid Mech.* **172**, 307–320.
- TOWNSEND, A. A. 1956 *The Structure of Turbulent Shear Flow*, 1st edn. Cambridge University Press.
- TOWNSEND, A. A. 1976 *The Structure of Turbulent Shear Flow*, 2nd edn. Cambridge University Press.



Minerva Access is the Institutional Repository of The University of Melbourne

**Author/s:**

Jones, M. B.;MARUSIC, IVAN;Perry, A. E.

**Title:**

Evolution and structure of sink-flow turbulent boundary layers

**Date:**

2001

**Citation:**

Jones, M. B., Marusic, I., & Perry, A. E. (2001). Evolution and structure of sink-flow turbulent boundary layers. *Journal of Fluid Mechanics*, 428, 1-27.

**Publication Status:**

Published

**Persistent Link:**

<http://hdl.handle.net/11343/34785>